Electronic Supplementary Information

Heterogeneity in a Metal–Organic Framework in-situ Guides Engineering Co@CoO Heterojunction for Electrocatalytic H_2 Production in tandem with Glucose Oxidation

Mengchen Wu [a], Jing Zhao [a], Congling Li [b] and Rui Liu [a]*

a. Shanghai Key Lab. of D&A for Metal-Functional Materials, School of Materials Science and Engineering, Tongji University, Shanghai 201804, China

Email: ruiliu@tongji.edu.cn

b. College of Chemistry and Chemical Engineering, Shanghai University of Engineering Science, Shanghai 201620, China

Experimental details

Materials characterization

The morphology of materials was observed on field emission scanning electron microscope (Hitachi, S-4800) and transmission electron microscope (JEM-2100F). X-ray Diffraction Spectrometry (XRD, D8ADVANCE) with Cu Kα line was used to analyze the phase. Fourier transform infrared (FTIR) spectra and X-ray photoelectron spectroscopy (XPS) were conducted on Nicolet NEXUS-470 spectrometer and Axis Ultra DLD, respectively. Nitrogen sorption isotherms were measured by Quadrachrome adsorption instrument (Autosorb-iQ3). BrunauerEmmett-Teller (BET) method and the Barrett-Joyner-Halenda (BJH) model were resorted for the specific surface area and pore size distribution.

Electrochemical Measurements

To prepare the catalyst ink, 10 mg sample was dispersed in 1250 μL of ethanol and 30 μL of 5% Nafion. 6μL ink was dropped onto the working electrode. The load mass of catalyst was calculated to be 0.23 mg cm^{-2}. The Tafel slope was calculated as: $\eta=blog(j)+a$, where η, j and b stand for overpotential, current density, and Tafel slope, respectively.

EIS spectra were tested in a frequency range of 0.1 Hz ~100 kHz. Electrocatalytic stability was assessed by chronoamperometry (CA) method. Electrochemical double layer capacitance (C_{dl}) was evaluated by

CV method. Electrochemical active surface area (ECSA) for the catalyst was calculated from C_{dl} as : ECSA = $C_{dl}/C_{s,}$ where C_s usually takes the value of 20-60 µF cm^{-2}.

Before the quantification of H_2, a known amount (400, 900 and 1600 ppm) of H_2 standard gas was injected into the same cell with the same electrolyte solution volume and head space volume. It was then plotted as a function of the corresponding peak area in GC. Calibration curves were obtained by linear fitting of the as-obtained data points (Fig. S16).

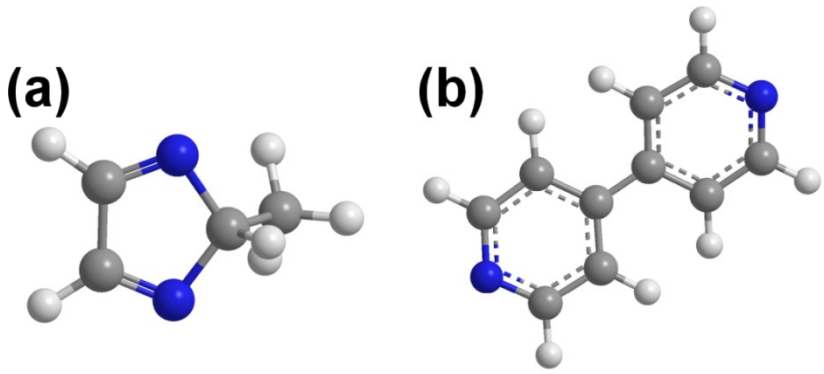

Fig. S1 Molecular structures of 2-methylimidazole and 4,4’-bipyridine (The N, C and H atoms are marked in blue, gray and white).

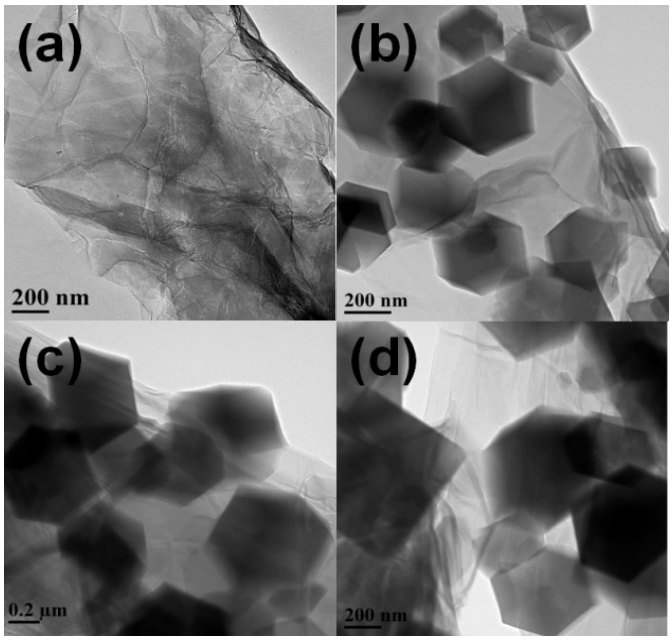

Fig. S2 TEM images of (a) Co^{2+}-Bpy/GO, (b) ZIF-67/GO, (c) ZIF-67-1/GO and (d) ZIF-67-3/GO.

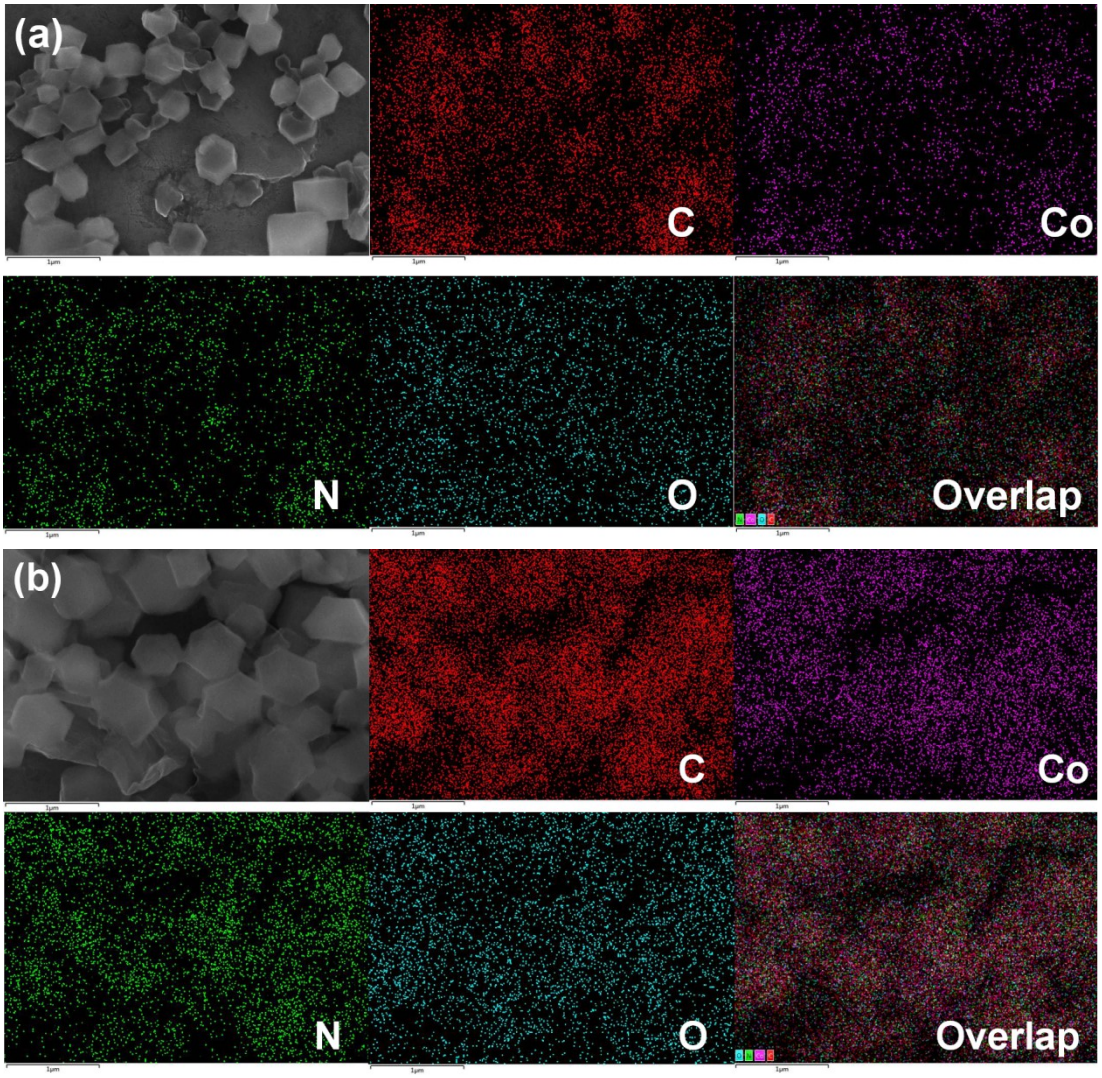

Fig. S3 SEM and corresponding element mapping images of (a) ZIF-67/GO and (b) ZIF-67-1/GO.

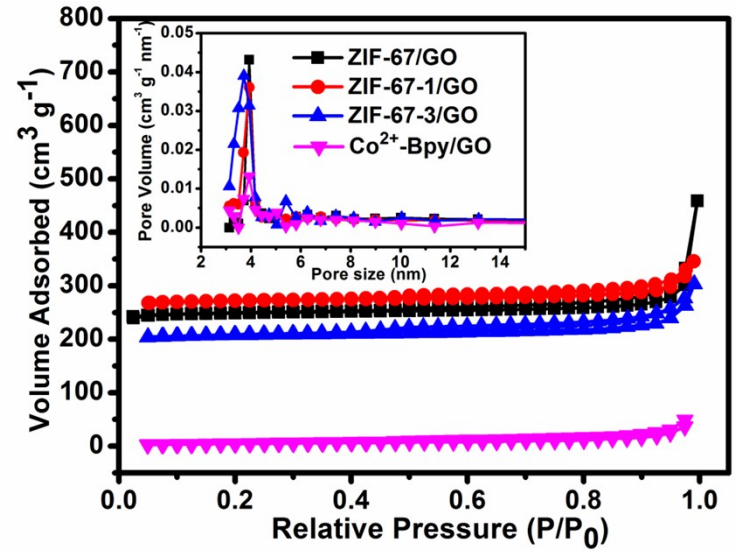

Fig. S4 N_2 sorption isotherms of ZIF-67/GO, ZIF-67-1/GO, ZIF-67-3/GO and Co^{2+}-Bpy/GO (Inset: pore size distribution).

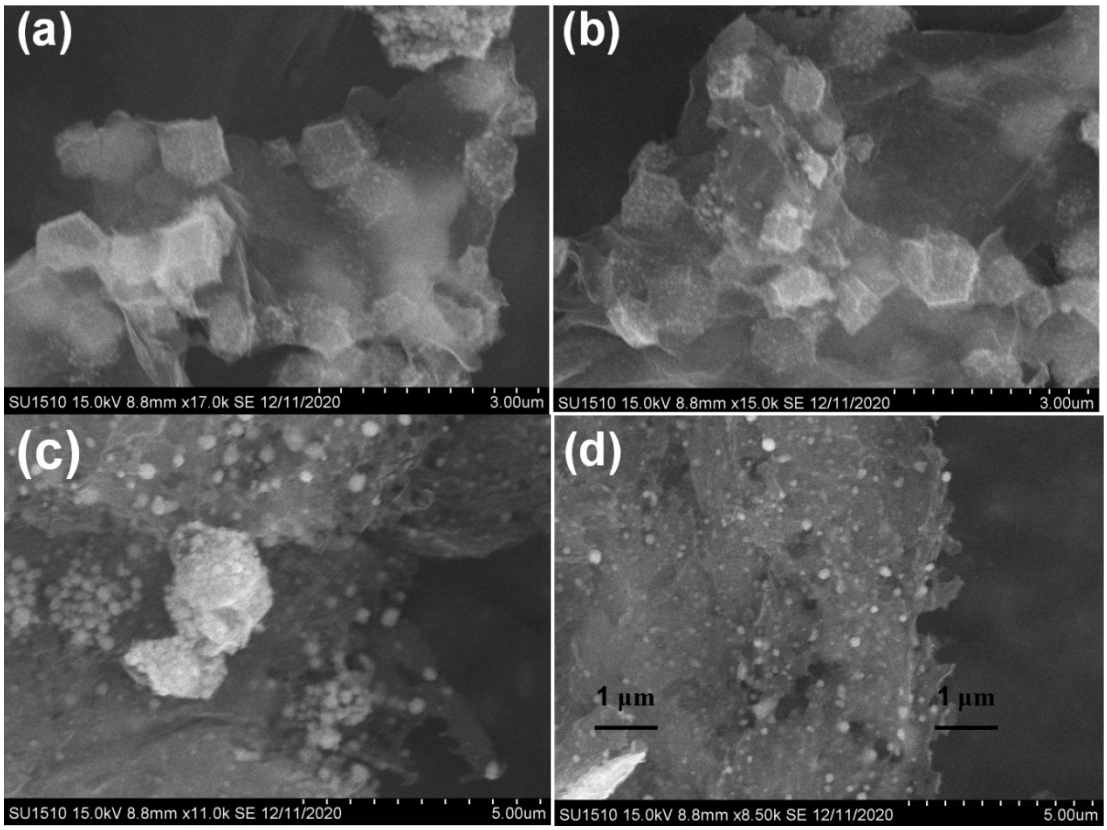

Fig. S5 SEM images of (a) Co/rGO, (b) Co@CoO-1/rGO, (c) Co@CoO-3/rGO and (d) CoO/rGO.

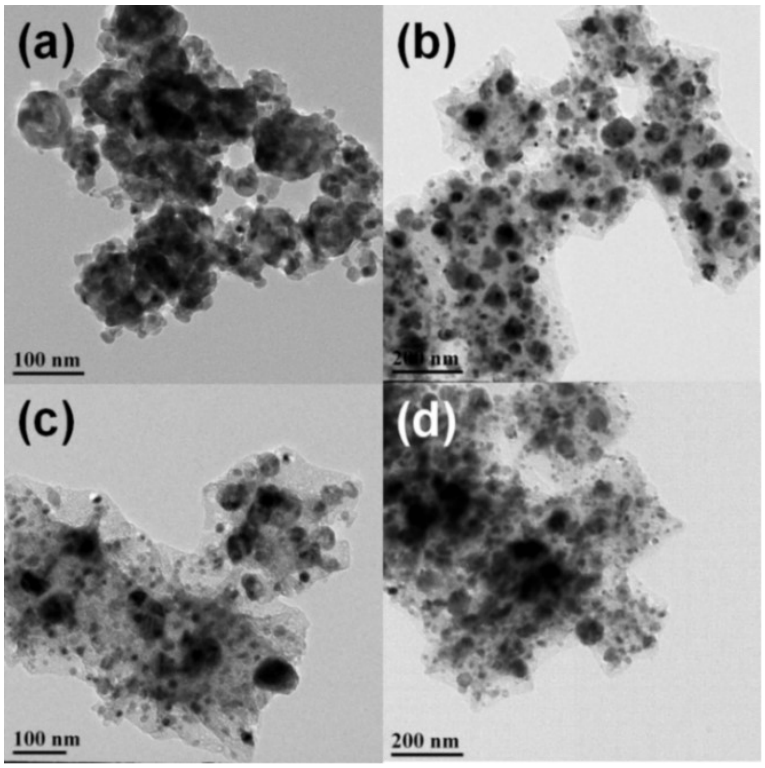

Fig. S6 TEM images of (a) Co_3O_4/rGO, and (b-d) corresponding carbon derivatives from ZIF-67, ZIF-67-1 and ZIF-67-3, respectively.

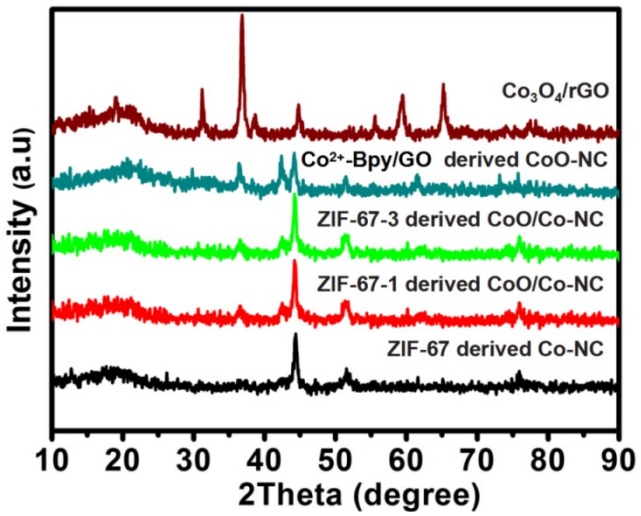

Fig. S7 XRD patterns of Co_3O_4/rGO and the carbon derivatives from Co^{2+}-Bpy/GO, ZIF-67-3, ZIF-67-1 and ZIF-67, respectively.

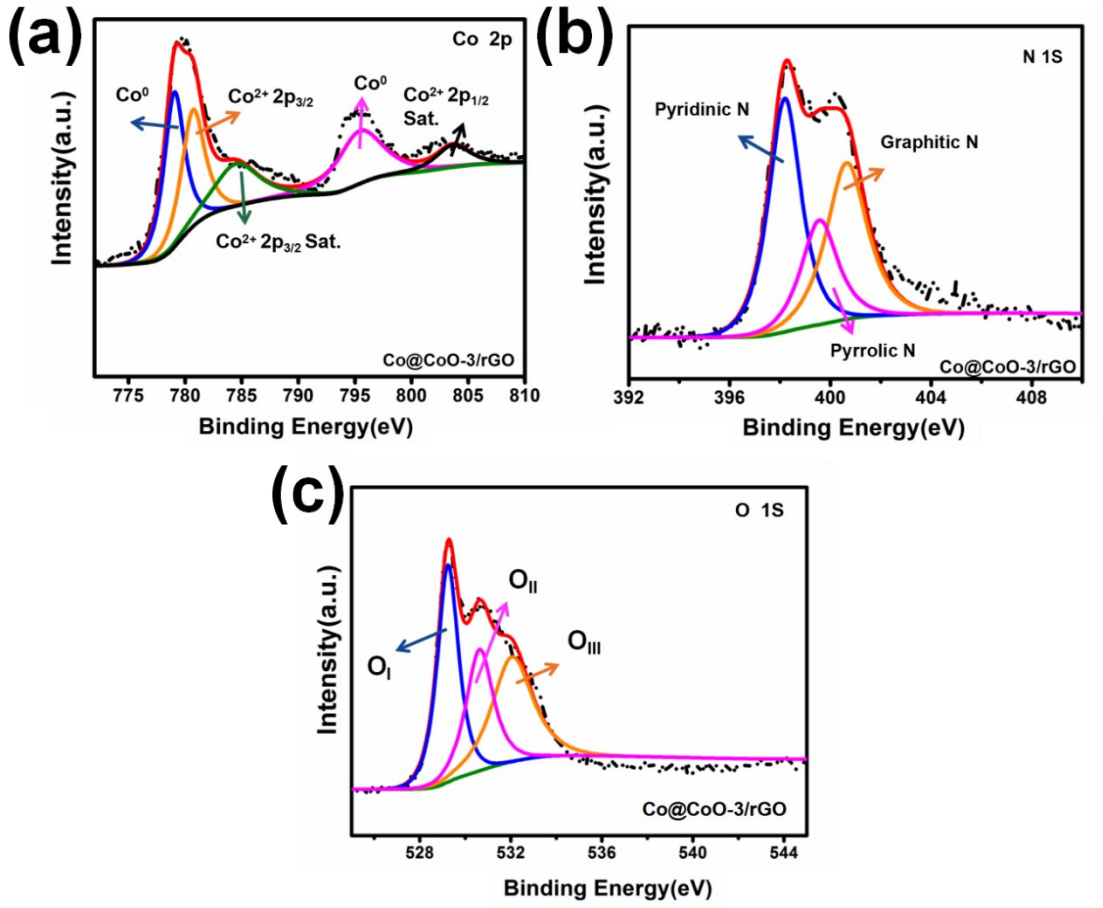

Fig. S8 XPS spectra of (a) Co 2p, (b) N 1s and (c) O 1s in Co@CoO-3/rGO.

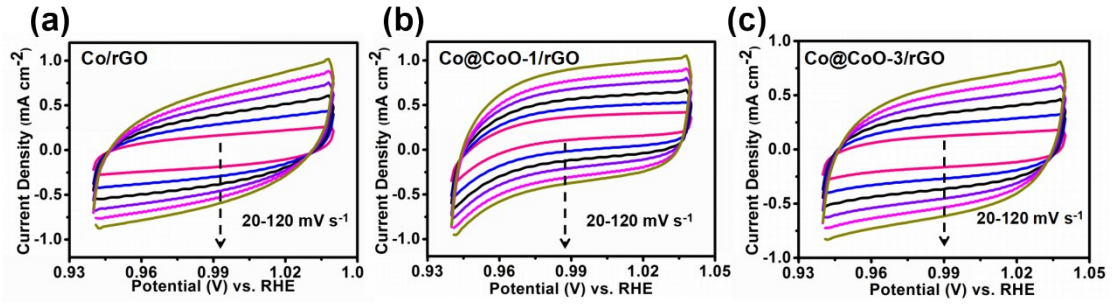

Fig. S9 CV curves of (a) Co/rGO, (b) Co@CoO-1/rGO and (c) Co@CoO-3/rGO at different scan rates.

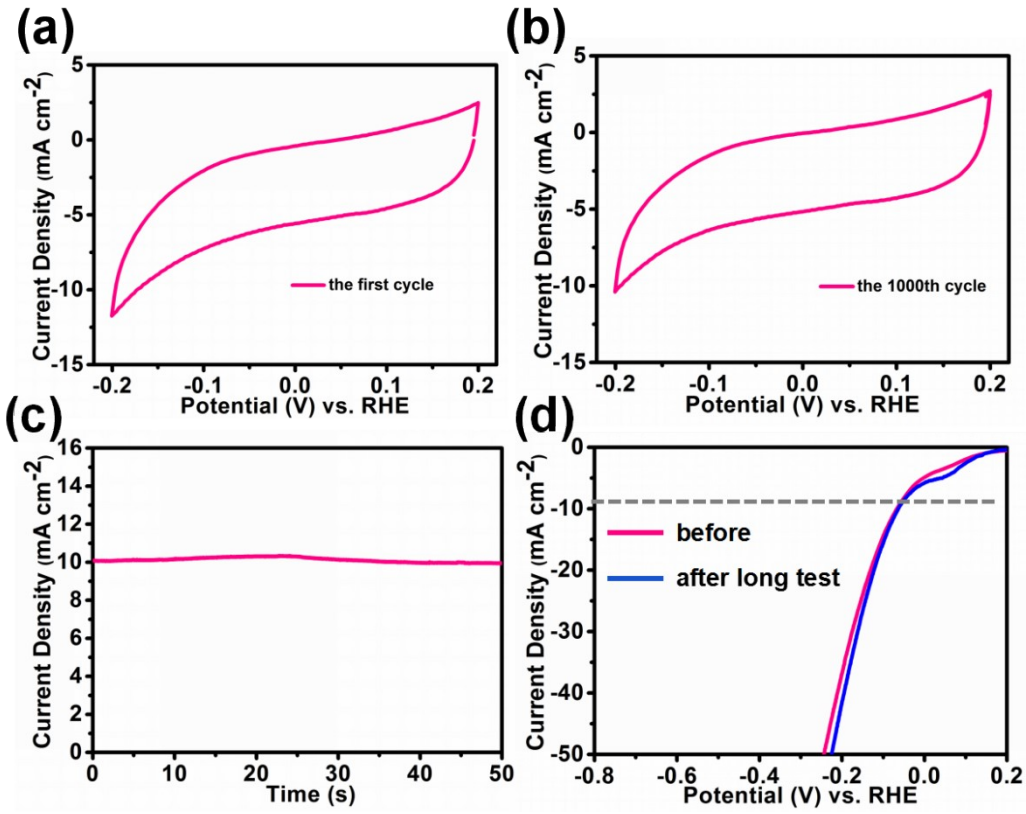

Fig. S10 (a,b) CV curves of Co@CoO-1/rGO during 1000 cycles, with a potential of 0.2~-0.2 V. (c) Stability test by chronoamperometry measurement at overpotential of -0.12 V for Co@CoO-1/rGO. (d) LSV curves of Co@CoO-1/rGO before and after long test.

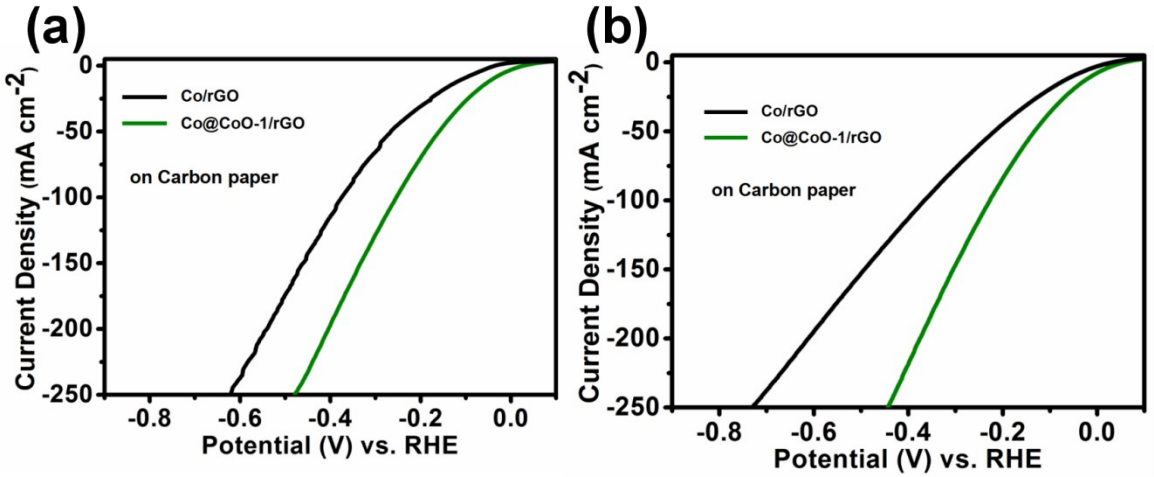

Fig. S11 Comparison of HER activities of Co@CoO-1/rGO and Co/rGO on carbon paper (a) before and (b) after stability test for 15h.

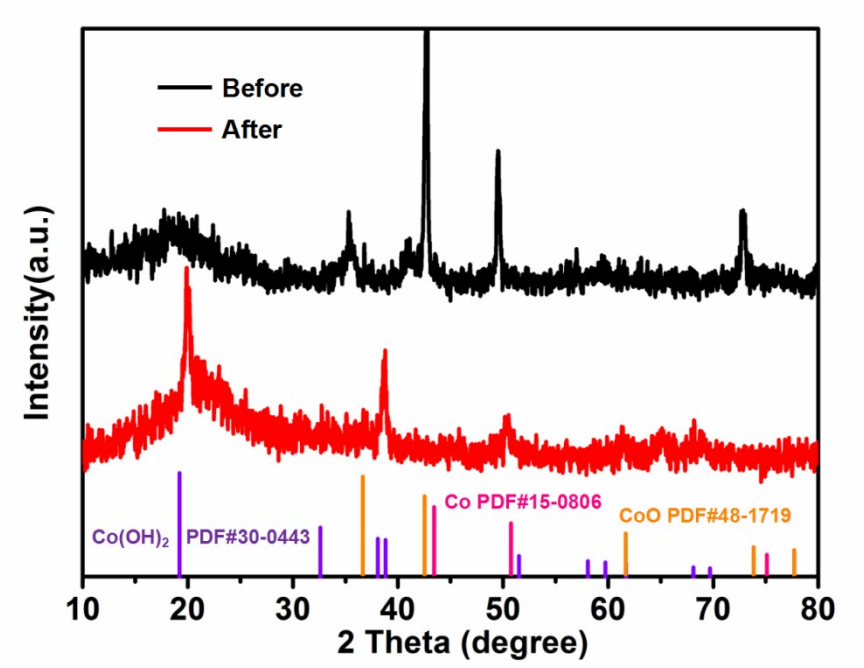

Fig. S12 Comparison of XRD patterns of Co@CoO-1/rGO before and after HER on carbon paper electrode.

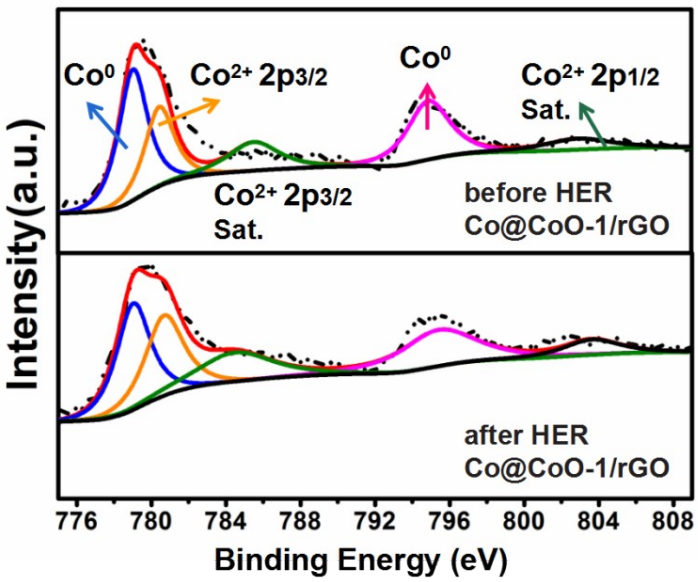

Fig. S13 Comparison of Co2p spectra of Co@CoO-1/rGO before and after HER.

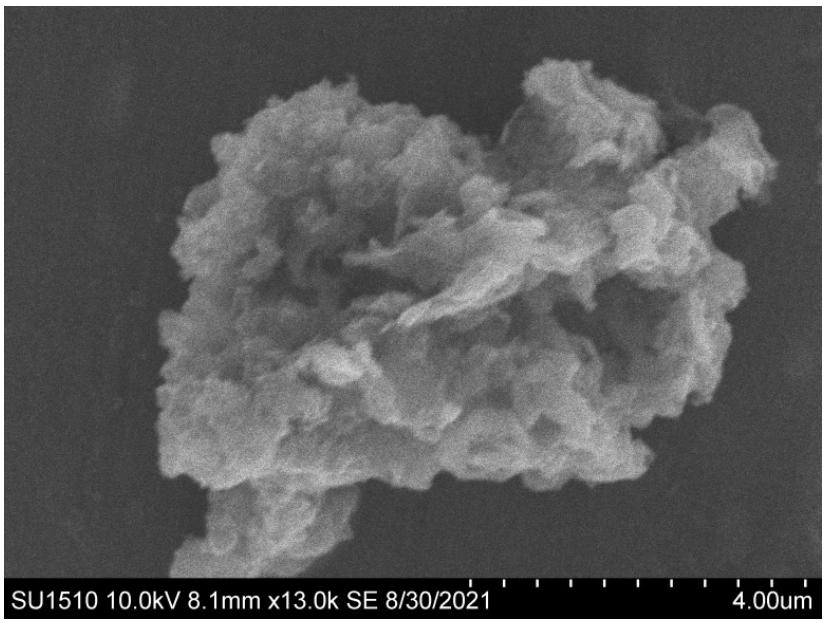

Fig. S14 SEM image of Co@CoO-1/rGO after HER.

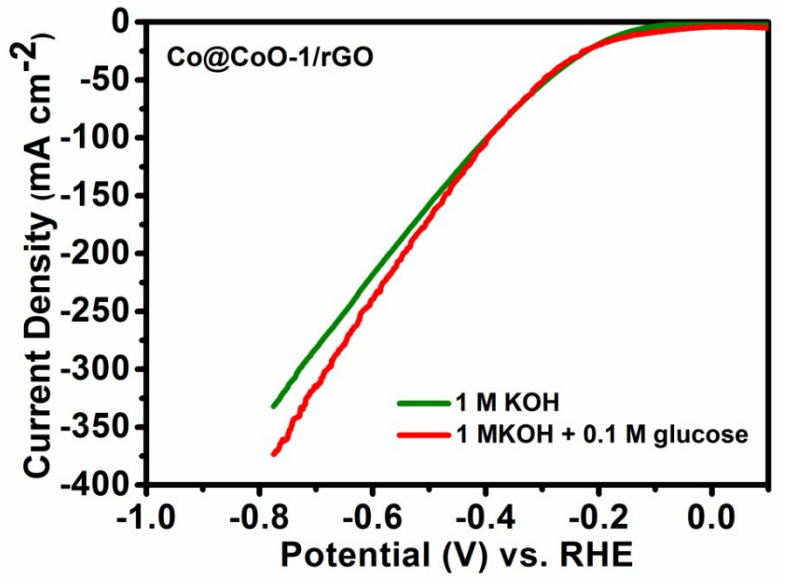

Fig. S15 LSV curves of Co@CoO-1/rGO in 1 M KOH with and without 0.1M glucose.

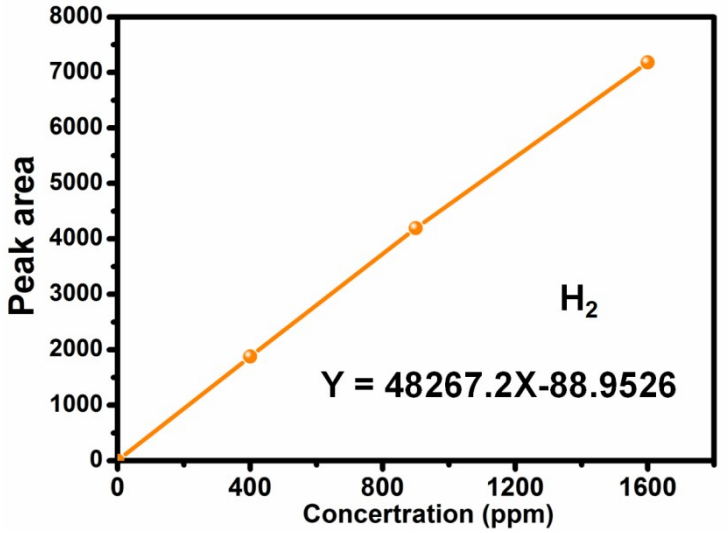

Fig. S16 Calibration curve of H_2.

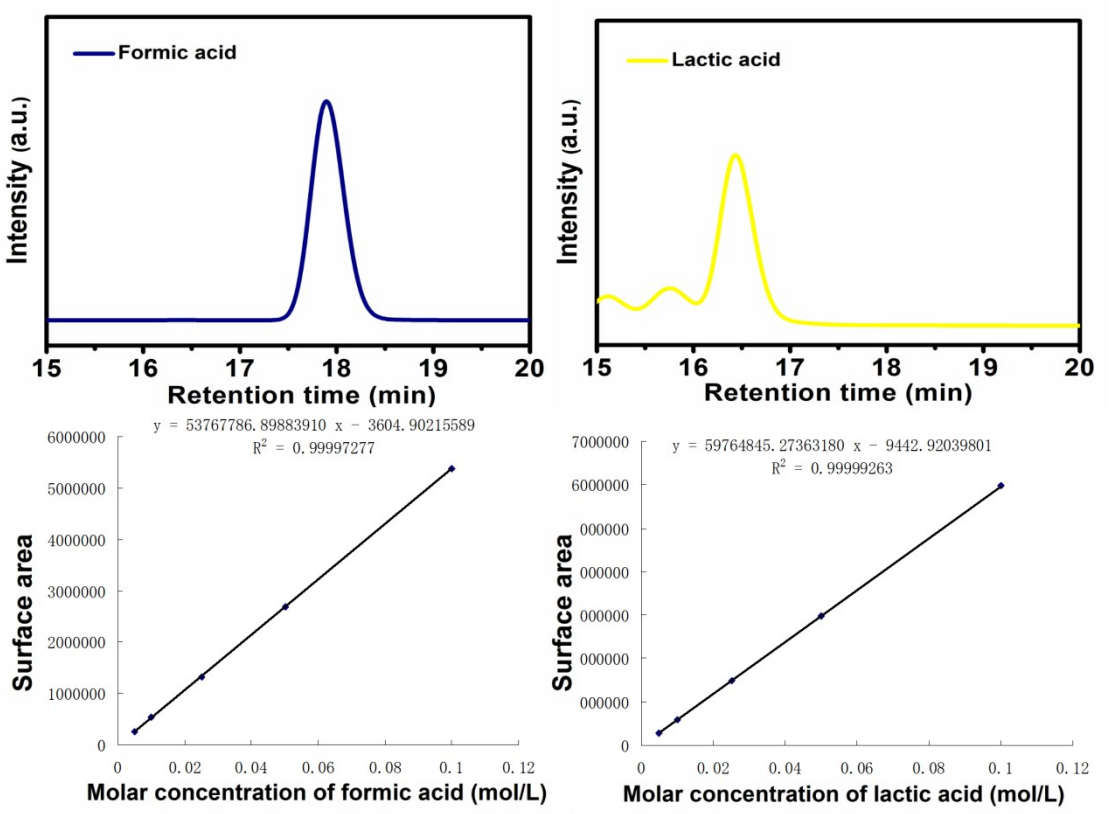

Fig. S17 HPLC measurements of pure lactic acid and formic acid, and their corresponding calibration curve.

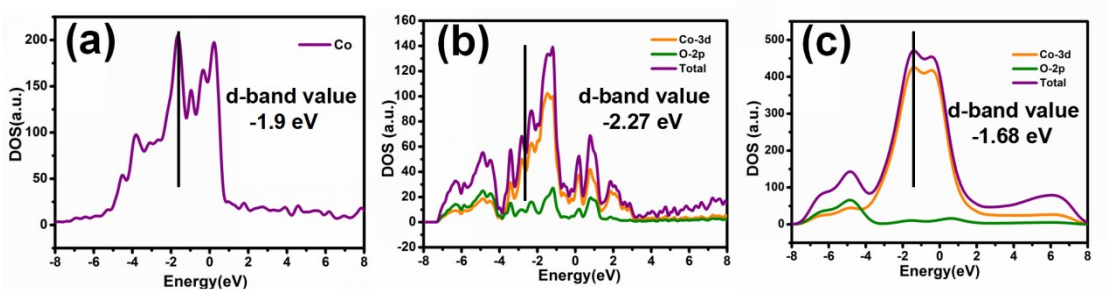

Fig. S18 Partial electronic density of states calculated for (a) Co, (b) CoO and (c) Co@CoO.

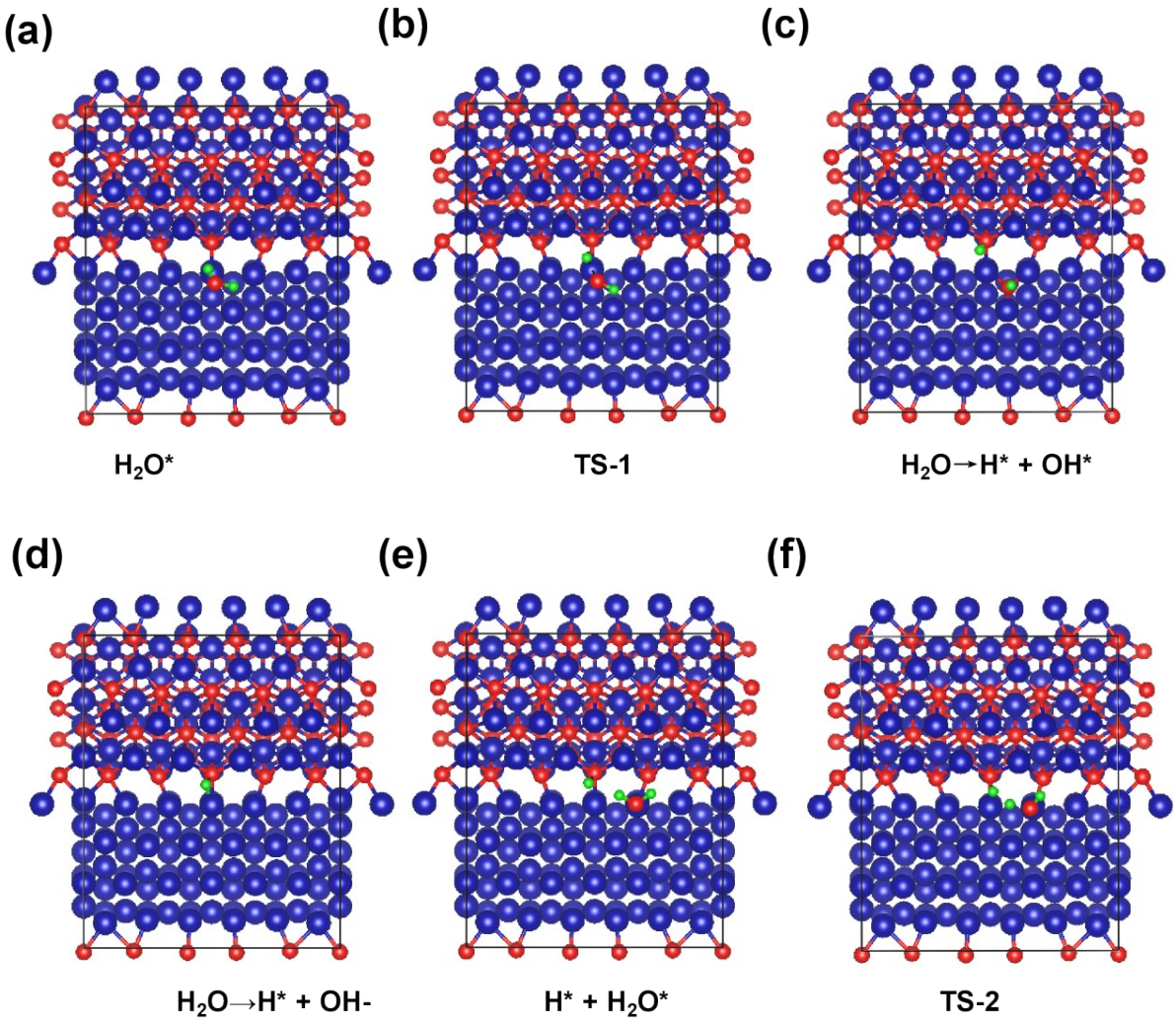

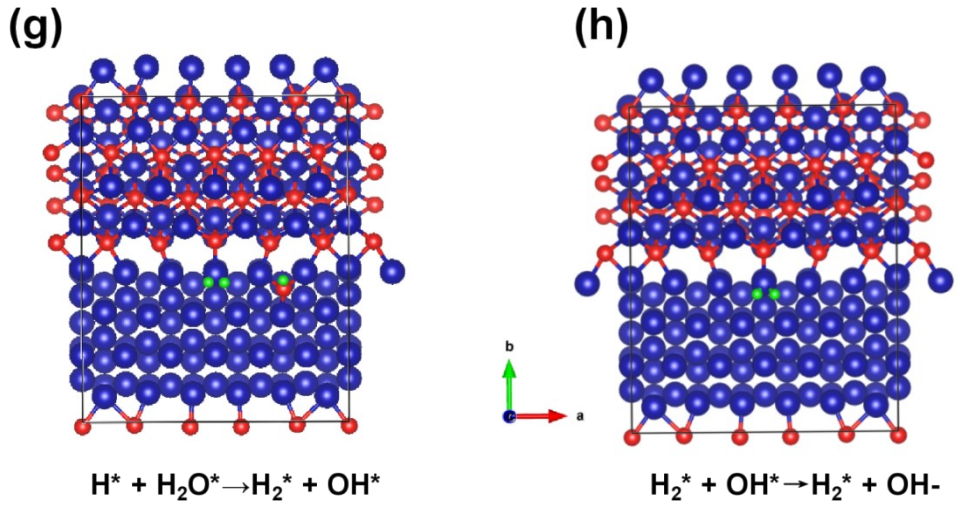

Fig. S19 (a-h) Adsorbed profiles of CoO during HER process. Co, O and H atoms are marked in blue, red and green.

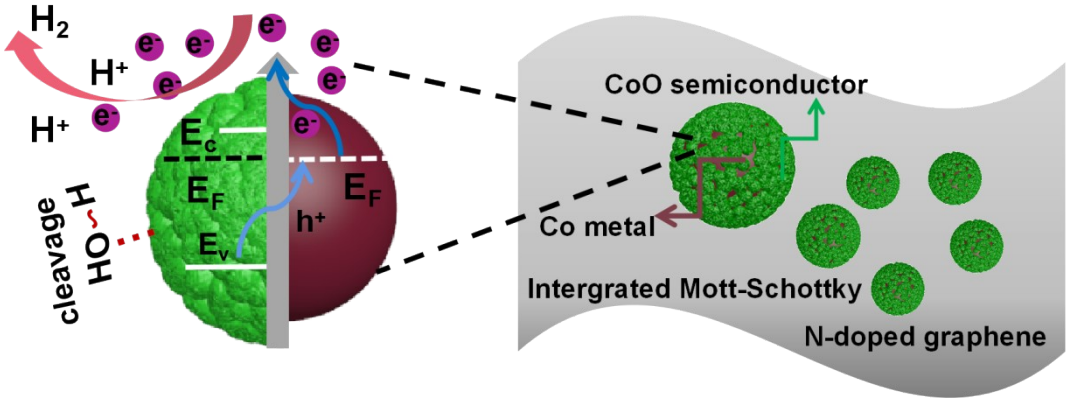

Fig. S20 Scheme of Volmer-Heyrovsky HER mechanism on Co@CoO Mott-Schottky heterojunctions.

Table S1 Content comparison (at. %) of Co@CoO-1/rGO before and after HER.

	Co	O	N
Before HER	2.36	8.53	5.31
After HER	2.01	14.62	5.16